Dynamic phosphorylation of Hcm1 promotes fitness in chronic stress

Michelle M. Conti[1], Jillian P. Bail[1], Rui Li[1], Lihua Julie Zhu[1,2,3], Jennifer A. Benanti[1,*]

[1]Department of Molecular, Cell and Cancer Biology, University of Massachusetts Chan Medical School, Worcester, MA 01605.

[2]Department of Genomics and Computational Biology, University of Massachusetts Chan Medical School, Worcester MA 01605.

[3]Program in Molecular Medicine, University of Massachusetts Chan Medical School, Worcester MA 01605.

*Correspondence: jennifer.benanti@umassmed.edu

Summary

Cell survival depends upon the ability to adapt to changing environments. Environmental stressors trigger an acute stress response program that rewires cell physiology, downregulates proliferation genes and pauses the cell cycle until the cell adapts. Here, we show that dynamic phosphorylation of the yeast cell cycle-regulatory transcription factor Hcm1 is required to maintain fitness in chronic stress. Hcm1 is activated by cyclin dependent kinase (CDK) and inactivated by the phosphatase calcineurin (CN) in response to stressors that signal through increases in cytosolic Ca^{2+}. Expression of a constitutively active, phosphomimetic Hcm1 mutant reduces fitness in stress, suggesting Hcm1 inactivation is required. However, a comprehensive analysis of Hcm1 phosphomutants revealed that Hcm1 activity is also important to survive stress, demonstrating that Hcm1 activity must be toggled on and off to promote gene expression and fitness. These results suggest that dynamic control of cell cycle regulators is critical for survival in stressful environments.

Introduction

Cells are continuously exposed to stressors in the environment and must adapt to these challenges to survive and proliferate. Adaptation not only protects healthy cells from death, but conversely, it can promote the development of disease. For instance, cancer cells must adapt to stressful environments when they metastasize to distant sites[1], and fungal pathogens rely upon stress response pathways for survival within the host[2]. Despite the importance of this process, the long-term changes that cells must undergo to maintain fitness and proliferation when faced with chronic stress are poorly understood.

The acute stress response, which occurs immediately following exposure to an environmental stressor, is conserved from yeast to humans and includes a downregulation of protein synthesis and an upregulation of stress response genes[3,4]. In addition to these changes that impact cell physiology, cell cycle-regulatory genes are downregulated, and cells undergo a

transient cell cycle arrest[5,6]. After cells adapt to the new environment, the acute stress response is resolved and cells resume proliferation in the new environment, albeit at a reduced rate[7]. It is thought that it is important to pause cell division while cells undergo adaptation to promote long-term survival[8,9], however this has not been examined for most stressors.

Some stressors signal through an increase in cytosolic Ca^{2+} and coordinate the stress response program and cell cycle changes by activating the conserved Ca^{2+}-activated phosphatase calcineurin (CN)[10,11]. CN activation leads to a decrease in expression of cell cycle-regulatory genes and controls the length of cell cycle arrest, in combination with the stress activated MAPK Hog1/p38[12]. One direct target of CN in budding yeast is the S-phase transcription factor (TF) Hcm1[13]. Hcm1 is a forkhead family transcriptional activator which, like it's human homolog FoxM1, plays a crucial role in maintaining genome stability[14,15]. Hcm1 regulates expression of key cell cycle genes including histone genes, downstream cell cycle-regulatory TFs, and genes that regulate mitotic spindle function. As cells progress through the cell cycle, Hcm1 is activated by multisite phosphorylation by cyclin dependent kinase (CDK)[16]. CDK phosphorylates eight sites in the Hcm1 transactivation domain (TAD) to stimulate its activity and a three site phosphodegron in the N-terminus to trigger proteasomal degradation. Immediately following exposure to $CaCl_2$ or LiCl stress, two stressors that activate CN, CDK activity decreases, the activating phosphates on Hcm1 are specifically removed by CN, and expression of Hcm1 target genes decreases[12,13,17]. Whether or not Hcm1 inactivation is critical for cells to adapt and survive in the face of chronic stress is unknown.

Mutations within the Hcm1 TAD have been used to study the consequences of phosphorylation. Phosphomimetic mutations at all CDK phosphosites in the TAD generate a constitutively active protein that leads to increased expression of Hcm1 target genes[16]. In normal growth conditions this mutant provides a fitness advantage to cells, rendering them more fit than wild type (WT)[13,18]. This is a surprising result because advantageous mutations are expected to be selected for during evolution. However, the fact that activating phosphates are removed by CN

when cells are faced with stress suggests that dephosphorylation and inactivation of Hcm1 may be necessary for cells to survive in stressful environments.

Here, we investigated this possibility and found that cells expressing a constitutively active, phosphomimetic Hcm1 mutant lose their fitness advantage when exposed to LiCl stress for several days. To determine the optimal level of Hcm1 activity for fitness in this environment, we screened a collection of Hcm1 mutants that encompass all possible combinations of non-phosphorylatable and phosphomimetic mutations in the TAD, representing the entire spectrum of possible activity levels. Surprisingly, this screen revealed that almost all mutants were less fit when growing in stress compared to stress-free conditions. Moreover, Cks1-docking sites that stimulate Hcm1 activity by promoting processive phosphorylation by CDK became more important for fitness when cells were grown in chronic stress. Finally, mutants that have increased Hcm1 activity because proteasomal degradation is blocked, but retain dynamic phosphoregulation of the TAD, were more fit than WT cells in chronic stress. These results demonstrate that simple Hcm1 inactivation is not the mechanism by which cells survive in chronic stress; instead, dynamic regulation of the Hcm1 activity – obtained through a combination of phosphorylation by CDK and dephosphorylation by CN – is critical to maintain fitness.

Results

Expression of a phosphomimetic Hcm1 mutant decreases fitness in LiCl stress

CDK phosphorylates eight sites in the Hcm1 TAD to activate the protein during an unperturbed cell cycle. When cells are exposed to a CN-activating stressor such as $CaCl_2$ or LiCl, these phosphates are removed by the phosphatase CN[13,18] (Figure 1A). This dephosphorylation occurs rapidly after exposure to LiCl[13] and, notably, Hcm1 remains in a hypophosphorylated state after cells adapt to LiCl stress and resume cycling (Figure 1B). To determine if dephosphorylation of Hcm1 is necessary for cells to survive when faced with chronic LiCl stress, we utilized a

constitutively active phosphomimetic Hcm1 mutant, Hcm1-8E, in which each CDK site in the TAD is mutated to two glutamic acids (S/T-P to E-E) to mimic the charge of a phosphate[16,18]. The Hcm1-8E protein is more active than WT Hcm1 and, as a result, confers a fitness advantage to cells in a competitive growth assay in optimal growth conditions that lack environmental stressors. To determine the consequence of elevated Hcm1 activity in stress, we compared the fitness of cells expressing Hcm1-8E to cells expressing WT Hcm1, in the presence or absence of LiCl (Figure 1C-1D). As previously shown, *hcm1-8E* cells exhibited a fitness benefit in the absence of stress (Figure 1C). However, *hcm1-8E* cells lost their fitness advantage and displayed a modest fitness defect when cultured in medium containing LiCl (Figure 1D), supporting the possibility that cells need to inactivate Hcm1 to survive in the presence of chronic LiCl stress.

Hcm1 mutants with fixed phosphorylation states are less fit in LiCl stress

Hcm1 retains some phosphorylation when cells are grown for three days in LiCl (Figure 1B), suggesting that some activity may remain, and that a reduced level of Hcm1 activity might be optimal in stress. To test this hypothesis, we employed Phosphosite Scanning, a recently developed screening approach that can simultaneously determine the effects of hundreds of phosphosite mutations on cellular fitness[18]. In this approach, a collection of strains expressing different phosphomutant proteins are pooled and passaged together. The abundance of each mutant in the population is followed over time by deep sequencing and a selection coefficient is calculated, based on the change in abundance of each mutant over time relative to WT. Screening libraries of mutants with all possible combinations of unphosphorylatable and phosophomimetic mutations enables the determination of the contribution of each individual phosphosite to a fitness phenotype.

To determine how different levels of Hcm1 activity impact fitness in stress, we performed Phosphosite Scanning screens with a collection of mutants in which each CDK phosphosite (S/T-P) in the TAD is mutated to an unphosphorylatable alanine (A-P) or two glutamic acids (E-E), in

all possible combinations (A/E library, Figure S1A)[18]. In unstressed growth conditions, fitness values conferred by these Hcm1 mutants are highly correlated with the activity of each mutant and this collection of mutants represents the entire continuum of possible Hcm1 activities, from the completely inactive Hcm1-8A mutant (with all phosphosites mutated to A-P) to the Hcm1-8E mutant that has increased activity relative to WT[18]. To determine how each Hcm1 mutant impacts fitness in stress, these mutants were simultaneously screened in control and LiCl containing media (Figure 2A).

First, we examined how overall fitness was impacted when cells were growing in stress. Selection coefficients of each mutant in LiCl-containing medium were directly compared with those from control medium (Figure 2B). Surprisingly, although there was a strong correlation between selection coefficients in the two environments, almost all mutants were less fit in LiCl than control conditions. This effect was most severe for mutants with greatest number of phosphomimetic (activating) mutations (Figure 2C), whereas mutants that had two or fewer phosphomimetic mutations were most similar between control and LiCl media. Notably, although the *hcm1-8E* mutant displayed a modest fitness defect in pairwise competition assays carried out in LiCl (Figure 1D), it had a slight fitness advantage in pooled screens. This observation is likely due to technical differences in the experimental approach, and consistent with previous findings that pooled screens result in slightly higher selection coefficients than pairwise competition assays[18]. However, the *hcm1-8E* mutant fitness advantage was modest in pooled LiCl screens and decreased in LiCl compared to control conditions (Figure 2C, mutant with eight E substitutions). These data demonstrate that Hcm1 activity is required for fitness in stress, however the most highly active mutants exhibit large reductions in fitness compared to control growth conditions.

Next, we wanted to determine how individual TAD phosphosites impact cellular fitness in LiCl stress. To do this, we compared the selection coefficients of all mutants that had either a non-phosphorylatable alanine (A) or two glutamic acids (E) at each site (Figure 2D, 2E). In both control

and LiCl conditions, a phosphomimetic mutation at any site increased fitness relative to an alanine substitution at the same site. Notably, mutations at sites T460 and S471 had the greatest effect on fitness in both conditions, consistent with previous measurements in the absence of stress[18]. Together, these data show that when phosphorylation patterns of Hcm1 are fixed because all sites are changed to either phosphodeficient or phosphomimetic amino acids, the fitness of almost all mutants is decreased in stress. This raises the possibility that it is not inactivation of Hcm1 that is important for cells to maintain fitness in stress, but rather dynamic regulation conferred by phosphorylation and dephosphorylation of the TAD.

Elevated importance of processive Hcm1 phosphorylation in stress

To investigate the importance of dynamic phosphorylation of Hcm1 in stress, we used Phosphosite Scanning to screen libraries of mutants that include WT phosphosites in combination with phosphodeficient or phosphomimetic mutations. In contrast to the A/E library, in which all phosphosites are fixed, the inclusion of WT sites allows some phosphorylation by CDK during the experiment and can reveal how a fixed phosphorylation state at one site influences phosphorylation at other sites[18]. We screened two collections of mutants: one in which all sites are either WT or a non-phosphorylatable alanine (WT/A library, Figure S1B); and one in which all sites are either WT or phosphomimetic (WT/E library, Figure S1C)[18]. The fitness of all mutants was compared between control conditions and LiCl conditions, as described above.

First, we asked whether all eight sites in the TAD contribute to fitness in LiCl stress, by analyzing the results from the WT/A library screen. Similar to the A/E screen, selection coefficients for all mutants were correlated between control and LiCl stress, however all scores were reduced in LiCl compared to control (Figure S2A). Moreover, alanine substitutions in an otherwise WT background reduced fitness to a greater extent than observed when the same alanine substitutions were included an otherwise phosphomimetic background (compare Figure S2B with Figure 2C). This observation is consistent with a previous discovery that CDK relies upon the

157 phosphoadapter subunit Cks1 to promote phosphorylation of critical regulatory sites in the Hcm1
158 TAD[18]. Cks1 can only bind to phosphothreonine[19,20], so alanine substitutions reduce activity in two
159 ways: first, activity is directly reduced because alanines cannot be phosphorylated and provide
160 the charge conferred by a phosphate and second, activity is indirectly decreased because
161 alanines cannot interact with Cks1 and thereby reduce phosphorylation of more C-terminal WT
162 sites in the domain. Despite the decreased fitness of all mutants in the WT/A library, fitness
163 generally increased with the number of WT sites in any given mutant (Figure S2B), and a WT site
164 was more advantageous than an alanine at each position (Figure S2C, S2D), in both control and
165 LiCl conditions. These results support the conclusion that phosphorylation at each site contributes
166 to Hcm1 activity in both control and stress conditions.

167 We further explored the contribution of Cks1 priming sites to fitness in stress by screening
168 the WT/E library (Figure S1C). Like alanine mutations, phosphomimetic (E-E) mutations cannot
169 serve as Cks1 priming sites. Because of this, E-E substitutions effectively behave as separation
170 of function mutations: they contribute to Hcm1 activation because they are charged, but are
171 unable to act as Cks1 priming sites, so they impair phosphorylation of more C-terminal WT sites
172 in the TAD. The cumulative effect of these mutations is evident when comparing selection
173 coefficients of WT/E mutants in control and LiCl conditions (Figure 3A). Whereas most mutants
174 in this collection are more fit than WT in control conditions, the majority of mutants become less
175 fit than WT in stress (Figure 3A, lower right quadrant). The subset of mutants that remained more
176 fit than WT in stress included most mutants that have phosphomimetic mutations at T460 and
177 S471, likely because this group of mutants does not depend on Cks1 priming to facilitate the
178 phosphorylation of these two sites that have the greatest impact on Hcm1 activity (Figure 2D).
179 Notably, in the WT/E library, fitness did not increase with the number of phosphomimetic mutations
180 when cells were growing in LiCl (Figure 3B), suggesting that priming by Cks1 is of increased
181 importance when cells are growing in stress.

To further investigate the need for Cks1 priming, we analyzed the fitness of phosphomutants based on their genotype at each site. If a phosphomimetic mutation has a negative effect and confers a reduced selection coefficient compared to the WT CDK site, it suggests that position functions as a priming site[18]. For example, in control media mutants that are phosphomimetic at site 428 are less fit than mutants that are WT at the same site, indicating that site 428 is a Cks1 priming site (Figure 3C)[18] .Notably, this deleterious fitness effect was amplified in LiCl stress, and there was a similar reduction in fitness among mutants that are phosphomimetic at site 440 (Figure 3D). Interestingly, mutants that were phosphomimetic at two additional sites, 479 and 486, also showed a reduction in fitness relative to mutants that are WT at the same sites in LiCl. Since these phosphomimetic mutations improved or had little effect on fitness in control conditions (Figure 3C), it suggests that these may be additional Cks1 priming sites within the Hcm1 TAD that only become important for fitness in stress. In fact, mutants with phosphomimetic mutations at either T428 and T440 or T479 and T468 displayed significantly reduced fitness in stress compared to mutants with WT sites, despite equivalent fitness in control conditions (Figure 3E, 3F). The importance of Cks1-dependent priming supports the conclusion that dynamic phosphorylation of the Hcm1 TAD is critical for fitness when cells are challenged with LiCl stress.

Dynamic phosphorylation of the Hcm1 TAD is required for fitness in stress

If the *hcm1-8E* mutant is less fit in stress because its phosphorylation cannot be dynamically regulated, and not because it has increased activity, then an alternative mutant in which activity is increased by a different mechanism might not exhibit reduced fitness in stress. To test this possibility, we examined the fitness of *hcm1-3N* mutant cells. Hcm1-3N contains three alanine substitutions in the N-terminal phosphodegron that prevent proteasomal degradation and stabilize the protein, thereby increasing Hcm1 activity without perturbing TAD phosphorylation dynamics (Figure 4A)[16]. Cells expressing Hcm1-3N exhibit similar increases in fitness as Hcm1-8E

expressing cells, compared to WT, in the absence of stress (Figure 4B, 1C, 4F)[13,18]. Importantly, the Hcm1-3N mutant contains a WT TAD, so phosphorylation is reduced in chronic stress, despite increased Hcm1 protein levels (Figure S3A, S3B). If it is dynamic regulation of Hcm1 that is important for fitness in stress, *hcm1-3N* cells should differ from *hcm1-8E* and retain their fitness advantage.

To test this hypothesis, pairwise competition assays were carried out between *hcm1-3N* and WT cells in control and LiCl containing medium. Consistent with previous observations, *hcm1-3N* cells were more fit than WT cells in control conditions (Figure 4B, 4F). Notably, in contrast to the decreased fitness observed in *hcm1-8E* cells (Figure 1D, 4F), the fitness benefit in *hcm1-3N* cells was enhanced when cells were challenged with LiCl stress (Figure 4C, 4F). To compare these effects directly, these two sets of mutations were combined to generate a stable, constitutively active mutant (*hcm1-3N8E*, Figure 4A). In a pairwise competition assay, *hcm1-3N8E* cells had similar fitness as *hcm1-3N* cells in control conditions (Figure 4D), as previously reported[18]. However, *hcm1-3N8E* cells were less fit than *hcm1-3N* in LiCl stress (Figure 4E). Therefore, preventing dynamic phosphorylation reverses the fitness benefit provided by increased Hcm1 expression in stress.

When cells are continuously exposed to a CN-activating stress, cells experience bursts in cytosolic Ca^{2+}, followed by pulses of CN activity[21,22]. This suggests that Hcm1 may undergo pulses of inactivation in chronic stress, which could then be reversed by CDK activity. For some TFs, increasing the frequency of activation results in a greater induction of target gene expression, compared to increasing the amplitude of TF activity[23,24]. Therefore, we considered that Hcm1 may undergo pulses of activity in stress, through modulation of phosphorylation, which in turn could impact the expression of its target genes. If so, *hcm1-8E* cells may be unable to activate target genes to the same extent as *hcm1-3N* when exposed to stress. To test this hypothesis, cells expressing WT Hcm1, Hcm1-3N or Hcm1-8E were grown in control medium or LiCl for 40 hours and Hcm1 target gene expression was quantified by RNA sequencing. Hcm1 only activates target

gene expression during S-phase. Consequently, because the experiment was performed in asynchronous cultures, where only ~16% of cells are in S-phase (Figure S3C), we observed modest fold change differences between wild type and mutant strains for individual Hcm1 target genes (Dataset S2). For this reason, we used Gene Set Enrichment Analysis (GSEA) to examine changes in expression of Hcm1 target genes as a group. GSEA revealed that Hcm1 targets were collectively expressed at elevated levels in both *hcm1-3N* and *hcm1-8E* mutants compared to WT in unstressed conditions, confirming that the two mutants exhibit a similar increase in activity (Figure 4G, a negative normalized enrichment score (NES) indicates lower expression in WT compared to mutant). However, when cells were grown in LiCl, Hcm1 target genes increased in expression in *hcm1-3N* cells, but not in *hcm1-8E* cells. Moreover, target genes were more highly expressed in *hcm1-3N* cells than *hcm1-8E* cells when they were directly compared (Figure 4G). These results demonstrate that dynamic phosphorylation of Hcm1 in stress increases expression of Hcm1 target genes and suggests that expression of these genes promotes fitness in stress.

Discussion

Immediately upon exposure to an environmental stressor, cells rewire many cellular pathways to promote stress resistance and long-term survival. A conserved feature of this acute response is the inactivation of cell cycle-regulatory TFs and downregulation of their target genes. Although cell cycle arrest is not required for the execution of the acute stress response[9], it is possible that arrest and/or downregulation of cell cycle-regulatory genes is important for adaptation and survival after cells resume proliferation in the new environment. In support of this possibility, we found that expression of the Hcm1-8E phosphomimetic mutant, which cannot be dephosphorylated and inactivated, reduces fitness in chronic LiCl stress (Figure 1D). However, several pieces of evidence argue that simple Hcm1 inactivation does not promote fitness in stress, but rather its phosphorylation must be dynamically regulated to activate target gene expression and ensure fitness. First, almost all Hcm1 phosphosite mutants that retain activity but have fixed

phosphorylation states are less fit in LiCl than control conditions (Figure 2B). This includes mutants that have WT-like activity, as well as those that have increased activity compared to WT. Second, TP motifs that function as Cks1 priming sites to promote processive phosphorylation by CDK are of greater importance in stress (Figure 3E, 3F), which suggests that increased CDK-dependent phosphorylation is required to counteract CN-dependent dephosphorylation. Finally, cells expressing the Hcm1-3N protein, which has increased activity because it is stabilized but retains phosphorylation-dependent activation[18], confers a fitness advantage in LiCl stress (Figure 4C). Together, these data demonstrate that Hcm1 activity is required for fitness in stress, and that its dynamic phosphoregulation is critical.

Dynamic regulation is a recognized feature of many TFs, most notably TFs that respond to stress. In mammalian cells pulsatile nuclear localization and activation of NFAT[25], p53[26–28] and NFκB[29–32] lead to an altered transcriptional output in response to different signals. In budding yeast, at least ten TFs display pulsatile nuclear localization in response to specific cues, thereby increasing frequency of their activation[33]. In the case of the stress-activated TF Msn2, exposure to distinct stressors triggers either sustained or pulsatile Msn2 nuclear localization[34], resulting in expression of distinct groups of target genes belonging to different promoter classes[23,24]. Notably, the CN-regulated TF Crz1 also exhibits pulsative activation via regulation of its nuclear localization[21,22]. When cells are exposed to continuous extracellular $CaCl_2$, the frequency of cytosolic Ca^{2+} pulses increases, and these are followed by pulses of CN activation. CN then dephosphorylates Crz1, leading to pulses of nuclear localization and target gene activation. Importantly, Hcm1 does not display pulses of nuclear localization[33], instead its activation is controlled by phosphorylation. Since Hcm1 is also a CN target, we propose that when cells are growing in LiCl stress pulses of CN activity result in dephosphorylation and inactivation of Hcm1, which are then countered by CDK-dependent phosphorylation, leading to pulses of Hcm1 activity. To our knowledge the only described mechanism of TF frequency modulation is through changing

TF localization, therefore dynamic phosphorylation represents a novel mechanism of controlling TF target gene expression in stress.

Dynamic phosphoregulation is likely to also control the activities of other CDK target proteins in stress. In addition to CN, which antagonizes CDK as well as other kinases[11], the cell cycle-regulatory phosphatase Cdc14 is activated during the stress response[35–37] and could regulate phosphorylation dynamics. Moreover, a recent phosphoproteomic study monitored proteome-wide phosphorylation after acute exposure to more than 100 stress conditions and found that ~20% of phosphorylated proteins show a change in phosphorylation after acute stress exposure[38]. However, monitoring dynamic changes in phosphorylation status has largely been restricted to proteins that undergo a localization change or other easily measurable phenotype. Here, we show that Phosphosite Scanning can be used to reveal the importance of phosphorylation dynamics[18]. Screening mutants in which all sites are mutated to either non-phosphorylatable or phosphomimetic mutations reveals the importance of being able to add and remove phosphates. In addition, by screening mutants that combine phosphosite mutations and wild type sites, Phosphosite Scanning can reveal whether priming sites for the CDK accessory subunit Cks1 are important in stress, supporting the importance of dynamic phosphorylation. We anticipate that this approach will enable the investigation of phosphorylation dynamics of other proteins and reveal whether dynamic phosphorylation is a common mechanism that modulates protein function when cells are growing in stressful environments.

Methods

Yeast strains and plasmids

All cultures were grown in rich medium (YM-1) or synthetic media lacking uracil (C-Ura) with 2% dextrose or galactose. Cultures were grown at 30°C or 23°C as indicated. A record of strains and plasmids used in this study can be found in Tables S1 and S2, respectively.

Co-culture competition assays

Pairwise competition assays were done as described in Conti et al. 2023[18]. Strains in which the endogenous copy of *HCM1* is regulated by a galactose inducible promoter (*GAL1p-HCM1*) and expressing either WT or non-fluorescent GFP were transformed with plasmids expressing WT or mutant *HCM1* from the *HCM1* promoter. Initially, cultures were grown in synthetic media lacking uracil with 2% galactose to ensure expression of *HCM1*. Logarithmic phase cells were equally mixed by adding one optical density (OD600) of each strain to the same culture tube in a final volume of 10mL C-Ura with 2% galactose. To determine the starting abundance of each strain, 0.15 optical densities were collected from the co-culture tubes. Samples were pelleted by centrifugation, resuspended in 2mL sodium citrate (50mM sodium citrate, 0.02% NaN_3, pH 7.4) and stored at 4°C pending analysis by flow cytometry. To evaluate fitness in LiCl stress, co-cultures were diluted within a range of 0.005-0.04 optical densities (OD_{600}) into synthetic media lacking uracil with 2% dextrose with or without 150mM LiCl after mixing at the start of the experiment. Cultures were then sampled and diluted every 24 hours for a total of 96 hours. Cultures reached saturation prior to dilution. At each timepoint, 0.15 optical densities were collected, pelleted, and resuspended in 2mL sodium citrate, and stored at 4°C until the conclusion of the experiment. Following the final timepoint, the percentage of GFP positive cells was quantified in each sample using a Guava EasyCyte HT flow cytometer and GuavaSoft software. 5000 cells were measured in all samples. Results were analyzed using FloJo software. Averages of n=3-13 biological replicates are shown, exact number is indicated in the figure legends. Selection coefficients for pairwise assays were calculated by calculating the slope of the best fit line of log2 fold change in mutant fraction over time, relative to WT in the same experiment.

Western blotting

Yeast culture amounting to one optical density (OD600) was collected, pelleted by centrifugation, and stored at -80°C prior to lysis. Cell pellets were lysed by incubation with cold TCA buffer (10mM Tris pH 8.0, 10% trichloroacetic acid, 25mM ammonium acetate, 1mM EDTA) on ice for 10 minutes. Lysates were mixed by vortexing and pelleted by centrifugation at 16,000xg for 10 minutes at 4°C. The supernatant was aspirated, and cell pellets were resuspended in 75μL resuspension solution (100mM Tris pH 11, 3% SDS). Lysates were incubated at 95°C for five minutes then allowed to cool to room temperature for five minutes. Lysates were clarified by centrifugation at 16,000xg for 30 seconds at room temperature. Supernatants were then collected, transferred to a new tube and 25μL 4X SDS-PAGE sample buffer (250mM Tris pH 6.8, 8% SDS, 40% glycerol, 20% β-mercaptoethanol) was added. The samples were incubated at 95°C for five minutes, then allowed to cool to room temperature and stored at -80°C.

For standard Western blots, resolving gels contain 10% acrylamide/bis solution 37.5:1, 0.375M Tris pH 8.8, 0.1% SDS, 0.1% ammonium persulfate (APS), 0.04% tetremethylethylenediamine (TEMED). Phos-tag gels contain 6% acrylamide/bis solution 29:1, 386mM Tris pH 8.8, 0.1% SDS, 0.2% APS, 25μM Phos-tag acrylamide (Wako), 50μM manganese chloride and 0.17% TEMED. All stacking gels contain 5% acrylamide/bis solution 37.5:1, 126mM Tris pH 6.8, 0.1% SDS, 0.1% APS and 0.1% TEMED. All SDS-PAGE gels were run in 1X running buffer (200mM glycine, 25mM Tris, 35mM SDS). Phos-tag gels were washed twice with 1X transfer buffer containing 10mM EDTA for 15 minutes (150mM glycine, 20mM Tris, 1.25mM SDS, 20% methanol) and once with 1X transfer buffer for 10 minutes on a shaking platform with gentle agitation. All gels were transferred to nitrocellulose in cold 1X transfer buffer at 0.45A for two hours. After transfer, nitrocellulose membranes were blocked in a 4% milk solution for 30 minutes.

Western blotting was performed with primary antibodies that recognize a V5 epitope tag (Invitrogen, 1:1000 dilution) or PSTAIRE (P7962, Sigma, 1:10,000 dilution). Primary antibody incubations were done overnight at 4°C. Importantly, molecular weight makers are not shown with Phos-tag gels as they do not accurately reflect the molecular weight of proteins.

Phosphosite Scanning screens

Phosphosite scanning screens were carried out using pooled plasmid libraries that had been previously constructed[18] and transformed into a *GAL1p-HCM1* strain. A plasmid expressing WT *HCM1* was added to all libraries as a control. During transformation, cells were cultured in YM-1 containing 2% galactose to maintain expression of endogenous *HCM1.* Following transformation, cells were cultured overnight at 23°C in synthetic media lacking uracil (C-Ura) with 2% galactose. After approximately 16 hours, an aliquot of transformed cells was removed and plated on C-Ura to confirm a transformation efficiency of at least 10X library size. Remaining cells were washed with 15mL C-Ura with 2% galactose five times, resuspended in 50mL C-Ura with 2% galactose and allowed to grow to logarithmic phase for approximately 48 hours at 30°C. The starting population was sampled to determine the initial abundance of each mutant in the population prior to selection. Cell pellets amounting to 20 optical densities were harvested, frozen on dry ice, and stored at -80°C prior to preparation of sequencing libraries. To evaluate fitness in stress, cultures were then diluted into synthetic media lacking uracil with 2% dextrose with or without 150mM LiCl after sampling at time zero. For all timepoints after time zero, cells were diluted into a range of 0.08 and 0.1 optical densities in 10mL of the appropriate media. At each timepoint, cultures reached saturation prior to sampling and dilution. Cultures were sampled and diluted as above every 24 hours for a total of 72 hours.

Illumina sequencing library preps

For analysis by sequencing, plasmids were recovered from the frozen samples using a YeaStar Genomic DNA Kit (Zymo Research). Mutant *hcm1* sequence was amplified by PCR (21 cycles) using plasmid specific primers and Phusion High-Fidelity DNA polymerase (New England Biolabs). DNA fragments were purified from a 1% agarose gel using a QIAquick Gel Extraction Kit (Qiagen). Barcoded TruSeq adapters were added to the mutant fragments by PCR (7 cycles) using primers specific to the *HCM1* region fused to either the TruSeq universal adapter or to a unique TruSeq indexed adapter. Sequences of oligonucleotides that were used in library construction can be found in Table S3. Barcoded fragments were purified from a 1% agarose gel as described above. Pooled barcoded libraries were sequenced on a HiSeq4000 platform (Novogene) to obtain paired-end 150 base pair sequencing reads. All sequencing data is available from the NCBI Sequencing Read Archive under BioProject # PRJNA1117860.

Phosphosite scanning data analysis

Abundance of *HCM1* alleles was quantified by counting all paired-end sequencing fragments that had an exact match to an expected sequence in both reads using a custom python script. Custom scripts used to generate count tables are available on GitHub (https://github.com/radio1988/mutcount2024/tree/main/AE_type) and Zenodo (https://zenodo.org/records/13144766). Selection coefficients were calculated as the slope of the log2 fraction of reads versus time for each mutant, normalized to the log2 fraction of reads versus time of WT. All selection coefficients for all screens can be found in Dataset S1. Box and whisker plots were generated using GraphPad Prism software. In all box and whisker plots the black center line indicates the median selection coefficient, boxes indicate the 25^{th}-75^{th} percentiles,

404 black lines represent 1.5 interquartile range (IQR) of the 25th and 75th percentile, black circles
405 represent outliers.

406

407 **RNA purification**

408 Cells amounting to five optical densities were harvested, pelleted by centrifugation at 3000rpm
409 for three minutes, and stored at -80°C. Cell pellets were then thawed on ice, resuspended in
410 400μL AE buffer (50mM sodium acetate pH 5.3, 10mM EDTA), and moved to room temperature.
411 40μL 10% SDS and 400μL AE equilibrated phenol was added to each sample and thoroughly
412 mixed by vortexing for 30 seconds. Samples were heated to 65°C for eight minutes and frozen in
413 a dry ice and ethanol bath for five minutes. Organic and aqueous layers were separated by
414 centrifugation at max speed for eight minutes at room temperature. The aqueous layer was then
415 transferred to a new tube. To remove any residual phenol, 500μL phenol:chloroform:isoamyl
416 alcohol was added and thoroughly mixed by vortexing for 30 seconds. Samples were incubated
417 at room temperature for five minutes and the aqueous and organic layers were separated by
418 centrifugation at maximum speed for five minutes at room temperature. The aqueous layer was
419 transferred to a new tube (~450μL) and the nucleic acids were precipitated by adding 40μL 3M
420 NaOAc pH 5.2 and 1mL 100% ethanol. Samples were mixed by vortexing for 15 seconds and
421 frozen in a dry ice and ethanol bath until completely frozen. Samples were then centrifuged at
422 maximum speed for 10 minutes at 4°C. Supernatants were decanted and pellets washed with 80%
423 ethanol and centrifuged at maximum speed for two minutes at 4°C. Supernatants were removed,
424 pellets allowed to dry completely and resuspended in 50μL water. DNA was degraded by
425 treatment with DNaseI. Samples were transferred to PCR strip tubes, 10μL 10X DNaseI buffer,
426 2μL DNaseI and 38μL water was added to each sample, and the samples were mixed by vortexing.
427 Samples were incubated at 30°C for 30 minutes, then cooled to 4°C in a thermocycler. 1μL 0.5M

EDTA was added to each sample and mixed. Samples were then heated to 75°C for 10 minutes and cooled to 4°C in a thermocycler. Purified RNA (100μL) was then transferred to a new tube and precipitated by adding 10μL sodium acetate pH 5.2 and 250μL 100% ethanol, and frozen in a dry ice and ethanol bath until completely frozen. RNA was then pelleted by centrifugation at maximum speed for 15 minutes at 4°C. Supernatants were decanted, the pellets washed with 80% ethanol, centrifuged at maximum speed for 2 minutes at 4°C. Supernatants were decanted and pellets allowed to air dry. Pure RNA was resuspended in water. Three biological replicates were performed. Library preparation and sequencing, including polyA mRNA selection, strand specific library preparation, and paired-end 100 base pair sequencing, were performed by Innomics/BGI Americas. All sequencing data is available in NCBI GEO and is accessible through GEO accession number GSE276435.

RNAseq analysis

RNASeq analysis was performed with OneStopRNAseq[39]. Paired-end reads were aligned to Saccharomyces_cerevisiae.R64-1-1, with 2.7.7a[40], and annotated with Saccharomyces_cerevisiae.R64-1-1.90.gtf. Aligned exon fragments with mapping quality higher than 20 were counted toward gene expression with featureCounts[41]. Differential expression (DE) analysis was performed with DESeq2[42]. Within DE analysis, 'ashr' was used to create log2 Fold Change (LFC) shrinkage [43] for all possible comparisons of WT and mutant strains, in both control and LiCl conditions. Significant DE genes (DEGs) were filtered with the criteria FDR < 0.05. Gene set enrichment analysis was performed for Hcm1 targets genes using GSEA[44] on the ranked LFC. GSEA results are included in Dataset S2.

Flow cytometry

To analyze DNA content by flow cytometry, cells amounting to 0.15 optical densities were collected, fixed in 70% ethanol and stored at 4°C. Cells were then pelleted by centrifugation at 3000rpm for three minutes, resuspended in 1mL sodium citrate buffer (50mM sodium citrate, 0.02% NaN_3, pH 7.4) and sonicated. Samples were then pelleted by centrifugation, resuspended in 1mL sodium citrate buffer containing 0.25mg/mL RNaseA, and incubated at 50°C for one hour. 12.5μL 10mg/mL Proteinase K was added to each tube and samples were incubated for an additional hour at 50°C. Following incubation, 1mL sodium citrate buffer containing 0.4μL Sytox green was added to each sample and samples were left at room temperature for 1 hour or 4°C overnight, protected from light, for staining. DNA content was analyzed on a Guava EasyCyte HT flow cytometer and GuavaSoft software. 5000 cells were measured in all samples. Results were analyzed using FloJo software.

Acknowledgements

The authors thank Tom Fazzio and members of the Benanti lab for insightful discussions and critical reading of the manuscript. This work was supported by National Institutes of Health grant R35GM136280 to J.A.B.

References

1. Senft, D., and Ronai, Z.A. (2016). Adaptive Stress Responses During Tumor Metastasis and Dormancy. Trends Cancer *2*, 429–442. https://doi.org/10.1016/j.trecan.2016.06.004.

2. Park, H.-S., Lee, S.C., Cardenas, M.E., and Heitman, J. (2019). Calcium-Calmodulin-Calcineurin Signaling: A Globally Conserved Virulence Cascade in Eukaryotic Microbial Pathogens. Cell Host Microbe *26*, 453–462. https://doi.org/10.1016/j.chom.2019.08.004.

3. Gasch, A.P., Spellman, P.T., Kao, C.M., Carmel-Harel, O., Eisen, M.B., Storz, G., Botstein, D., and Brown, P.O. (2000). Genomic Expression Programs in the Response of Yeast Cells to Environmental Changes. Mol. Biol. Cell *11*, 4241–4257. https://doi.org/10.1091/mbc.11.12.4241.

4. Causton, H.C., Ren, B., Koh, S.S., Harbison, C.T., Kanin, E., Jennings, E.G., Lee, T.I., True, H.L., Lander, E.S., and Young, R.A. (2001). Remodeling of Yeast Genome Expression in Response to Environmental Changes. Mol. Biol. Cell *12*, 323–337. https://doi.org/10.1091/mbc.12.2.323.

5. Yaakov, G., Duch, A., García-Rubio, M., Clotet, J., Jiménez, J., Aguilera, A., and Posas, F. (2009). The stress-activated protein kinase Hog1 mediates S phase delay in response to osmostress. Molecular biology of the cell *20*, 3572–3582. https://doi.org/10.1091/mbc.e09-02-0129.

6. Clotet, J., Escoté, X., Adrover, M.A., Yaakov, G., Garí, E., Aldea, M., Nadal, E. de, and Posas, F. (2006). Phosphorylation of Hsl1 by Hog1 leads to a G2 arrest essential for cell survival at high osmolarity. EMBO J. *25*, 2338–2346. https://doi.org/10.1038/sj.emboj.7601095.

7. Flynn, M.J., Harper, N.W., Li, R., Zhu, L.J., Lee, M.J., and Benanti, J.A. (2024). Calcineurin promotes adaptation to chronic stress through two distinct mechanisms. Mol. Biol. Cell, mbcE24030122. https://doi.org/10.1091/mbc.e24-03-0122.

8. Bonny, A.R., Kochanowski, K., Diether, M., and El-Samad, H. (2021). Stress-induced growth rate reduction restricts metabolic resource utilization to modulate osmo-adaptation time. Cell Reports *34*, 108854. https://doi.org/10.1016/j.celrep.2021.108854.

9. Ho, Y.-H., Shishkova, E., Hose, J., Coon, J.J., and Gasch, A.P. (2018). Decoupling Yeast Cell Division and Stress Defense Implicates mRNA Repression in Translational Reallocation during Stress. Current Biology *28*, 1–21. https://doi.org/10.1016/j.cub.2018.06.044.

10. Cyert, M.S., and Philpott, C.C. (2013). Regulation of cation balance in Saccharomyces cerevisiae. Genetics *193*, 677–713. https://doi.org/10.1534/genetics.112.147207.

11. Goldman, A., Roy, J., Bodenmiller, B., Wanka, S., Landry, C.R., Aebersold, R., and Cyert, M.S. (2014). The Calcineurin Signaling Network Evolves via Conserved Kinase-Phosphatase Modules that Transcend Substrate Identity. Mol. Cell. https://doi.org/10.1016/j.molcel.2014.05.012.

12. Leech, C.M., Flynn, M.J., Arsenault, H.E., Ou, J., Liu, H., Zhu, L.J., and Benanti, J.A. (2020). The coordinate actions of calcineurin and Hog1 mediate the stress response through multiple nodes of the cell cycle network. PLoS Genetics *16*, e1008600-27. https://doi.org/10.1371/journal.pgen.1008600.

13. Arsenault, H.E., Roy, J., Mapa, C.E., Cyert, M.S., and Benanti, J.A. (2015). Hcm1 integrates signals from Cdk1 and Calcineurin to control cell proliferation. Molecular biology of the cell *26*, 3570–3577. https://doi.org/10.1091/mbc.e15-07-0469.

14. Pramila, T., Wu, W., Miles, S., Noble, W.S., and Breeden, L.L. (2006). The Forkhead transcription factor Hcm1 regulates chromosome segregation genes and fills the S-phase gap in the transcriptional circuitry of the cell cycle. Genes & Development *20*, 2266–2278. https://doi.org/10.1101/gad.1450606.

15. Alvarez-Fernández, M., and Medema, R.H. (2013). Novel functions of FoxM1: from molecular mechanisms to cancer therapy. Frontiers in oncology *3*, 30. https://doi.org/10.3389/fonc.2013.00030.

16. Landry, B.D., Mapa, C.E., Arsenault, H.E., Poti, K.E., and Benanti, J.A. (2014). Regulation of a transcription factor network by Cdk1 coordinates late cell cycle gene expression. The EMBO Journal *33*, 1044–1060. https://doi.org/10.1002/embj.201386877.

17. Flynn, M.J., and Benanti, J.A. (2022). Cip1 tunes cell cycle arrest duration upon calcineurin activation. Proc National Acad Sci *119*, e2202469119. https://doi.org/10.1073/pnas.2202469119.

18. Conti, M.M., Li, R., Ramos, M.A.N., Zhu, L.J., Fazzio, T.G., and Benanti, J.A. (2023). Phosphosite Scanning reveals a complex phosphorylation code underlying CDK-dependent activation of Hcm1. Nat Commun *14*, 310. https://doi.org/10.1038/s41467-023-36035-9.

19. McGrath, D.A., Balog, E.R.M., Kõivomägi, M., Lucena, R., Mai, M.V., Hirschi, A., Kellogg, D.R., Loog, M., and Rubin, S.M. (2013). Cks confers specificity to phosphorylation-dependent CDK signaling pathways. Nature Structural & Molecular Biology *20*, 1407–1414. https://doi.org/10.1038/nsmb.2707.

20. Kõivomägi, M., Örd, M., Iofik, A., Valk, E., Venta, R., Faustova, I., Kivi, R., Balog, E.R.M., Rubin, S.M., and Loog, M. (2013). Multisite phosphorylation networks as signal processors for Cdk1. Nature Structural & Molecular Biology *20*, 1415–1424. https://doi.org/10.1038/nsmb.2706.

21. Hsu, I.S., Strome, B., Plotnikov, S., and Moses, A.M. (2019). A Noisy Analog-to-Digital Converter Connects Cytosolic Calcium Bursts to Transcription Factor Nuclear Localization Pulses in Yeast. G3: Genes, Genomes, Genet. *9*, 561–570. https://doi.org/10.1534/g3.118.200841.

22. Cai, L., Dalal, C.K., and Elowitz, M.B. (2008). Frequency-modulated nuclear localization bursts coordinate gene regulation. Nature *455*, 485–490. https://doi.org/10.1038/nature07292.

23. Hansen, A.S., and O'Shea, E.K. (2013). Promoter decoding of transcription factor dynamics involves a trade-off between noise and control of gene expression. Mol. Syst. Biol. *9*, 704–704. https://doi.org/10.1038/msb.2013.56.

24. Hansen, A.S., and O'Shea, E.K. (2015). Limits on information transduction through amplitude and frequency regulation of transcription factor activity. eLife *4*, e06559. https://doi.org/10.7554/elife.06559.

25. Yissachar, N., Sharar Fischler, T., Cohen, A.A., Reich-Zeliger, S., Russ, D., Shifrut, E., Porat, Z., and Friedman, N. (2013). Dynamic Response Diversity of NFAT Isoforms in Individual Living Cells. Mol. Cell *49*, 322–330. https://doi.org/10.1016/j.molcel.2012.11.003.

26. Lahav, G., Rosenfeld, N., Sigal, A., Geva-Zatorsky, N., Levine, A.J., Elowitz, M.B., and Alon, U. (2004). Dynamics of the p53-Mdm2 feedback loop in individual cells. Nat. Genet. *36*, 147–150. https://doi.org/10.1038/ng1293.

552 27. Batchelor, E., Loewer, A., Mock, C., and Lahav, G. (2011). Stimulus-dependent dynamics of
553 p53 in single cells. Mol. Syst. Biol. *7*, 488–488. https://doi.org/10.1038/msb.2011.20.

554 28. Purvis, J.E., Karhohs, K.W., Mock, C., Batchelor, E., Loewer, A., and Lahav, G. (2012). p53
555 dynamics control cell fate. Science (New York, NY) *336*, 1440–1444.
556 https://doi.org/10.1126/science.1218351.

557 29. Lee, T.K., Denny, E.M., Sanghvi, J.C., Gaston, J.E., Maynard, N.D., Hughey, J.J., and
558 Covert, M.W. (2009). A Noisy Paracrine Signal Determines the Cellular NF-κB Response to
559 Lipopolysaccharide. Sci. Signal. *2*, ra65. https://doi.org/10.1126/scisignal.2000599.

560 30. Ashall, L., Horton, C.A., Nelson, D.E., Paszek, P., Harper, C.V., Sillitoe, K., Ryan, S., Spiller,
561 D.G., Unitt, J.F., Broomhead, D.S., et al. (2009). Pulsatile Stimulation Determines Timing and
562 Specificity of NF-κB-Dependent Transcription. Science *324*, 242–246.
563 https://doi.org/10.1126/science.1164860.

564 31. Tay, S., Hughey, J.J., Lee, T.K., Lipniacki, T., Quake, S.R., and Covert, M.W. (2010).
565 Single-cell NF-κB dynamics reveal digital activation and analogue information processing.
566 Nature *466*, 267–271. https://doi.org/10.1038/nature09145.

567 32. Lee, R.E.C., Qasaimeh, M.A., Xia, X., Juncker, D., and Gaudet, S. (2016). NF-κB signalling
568 and cell fate decisions in response to a short pulse of tumour necrosis factor. Sci. Rep. *6*,
569 39519. https://doi.org/10.1038/srep39519.

570 33. Dalal, C.K., Cai, L., Lin, Y., Rahbar, K., and Elowitz, M.B. (2014). Pulsatile dynamics in the
571 yeast proteome. Current biology : CB *24*, 2189–2194. https://doi.org/10.1016/j.cub.2014.07.076.

572 34. Hao, N., and O'Shea, E.K. (2012). Signal-dependent dynamics of transcription factor
573 translocation controls gene expression. Nat. Struct. Mol. Biol. *19*, 31–39.
574 https://doi.org/10.1038/nsmb.2192.

575 35. Reiser, V., D'Aquino, K.E., Ee, L.-S., and Amon, A. (2006). The stress-activated mitogen-
576 activated protein kinase signaling cascade promotes exit from mitosis. Molecular biology of the
577 cell *17*, 3136–3146. https://doi.org/10.1091/mbc.e05-12-1102.

578 36. Chasman, D., Ho, Y.-H., Berry, D.B., Nemec, C.M., MacGilvray, M.E., Hose, J., Merrill, A.E.,
579 Lee, M.V., Will, J.L., Coon, J.J., et al. (2014). Pathway connectivity and signaling coordination in
580 the yeast stress-activated signaling network. Molecular systems biology *10*, 759–759.
581 https://doi.org/10.15252/msb.20145120.

582 37. Tognetti, S., Jiménez, J., Viganò, M., Duch, A., Queralt, E., Nadal, E. de, and Posas, F.
583 (2020). Hog1 activation delays mitotic exit via phosphorylation of Net1. Proceedings of the
584 National Academy of Sciences *1505*, 201918308–201918933.
585 https://doi.org/10.1073/pnas.1918308117.

586 38. Leutert, M., Barente, A.S., Fukuda, N.K., Rodriguez-Mias, R.A., and Villén, J. (2023). The
587 regulatory landscape of the yeast phosphoproteome. Nat. Struct. Mol. Biol. *30*, 1761–1773.
588 https://doi.org/10.1038/s41594-023-01115-3.

589 39. Li, R., Hu, K., Liu, H., Green, M.R., and Zhu, L.J. (2020). OneStopRNAseq: A Web
590 Application for Comprehensive and Efficient Analyses of RNA-Seq Data. Genes-basel *11*, 1165.
591 https://doi.org/10.3390/genes11101165.

592 40. Dobin, A., Davis, C.A., Schlesinger, F., Drenkow, J., Zaleski, C., Jha, S., Batut, P.,
593 Chaisson, M., and Gingeras, T.R. (2013). STAR: ultrafast universal RNA-seq aligner.
594 Bioinformatics *29*, 15–21. https://doi.org/10.1093/bioinformatics/bts635.

595 41. Liao, Y., Smyth, G.K., and Shi, W. (2014). featureCounts: an efficient general purpose
596 program for assigning sequence reads to genomic features. Bioinformatics *30*, 923–930.
597 https://doi.org/10.1093/bioinformatics/btt656.

598 42. Love, M.I., Huber, W., and Anders, S. (2014). Moderated estimation of fold change and
599 dispersion for RNA-seq data with DESeq2. Genome Biol *15*, 550.
600 https://doi.org/10.1186/s13059-014-0550-8.

601 43. Stephens, M. (2017). False discovery rates: a new deal. Biostat Oxf Engl *18*, 275–294.
602 https://doi.org/10.1093/biostatistics/kxw041.

603 44. Subramanian, A., Tamayo, P., Mootha, V.K., Mukherjee, S., Ebert, B.L., Gillette, M.A.,
604 Paulovich, A., Pomeroy, S.L., Golub, T.R., Lander, E.S., et al. (2005). Gene set enrichment
605 analysis: A knowledge-based approach for interpreting genome-wide expression profiles. Proc
606 National Acad Sci *102*, 15545–15550. https://doi.org/10.1073/pnas.0506580102.

607

608 **Figure Legends**

609 **Figure 1. Expression of a phosphomimetic Hcm1 mutant decreases fitness in LiCl stress**

610 (A) Hcm1 activity is regulated by cyclin-dependent kinase (CDK) and the phosphatase calcineurin
611 (CN). (B) Phos-tag and standard Western blots showing Hcm1 phosphorylation and expression
612 after the indicated number of hours in LiCl stress. Hcm1 was detected with an antibody that
613 recognizes a 3V5 tag, PSTAIRE is shown as a loading control. Representative blots from n=3
614 experiments are shown. (C-D) Strains with the indicated genotypes were co-cultured in control
615 media (C) or media with 150mM LiCl (D). Percentage of each strain was quantified by flow
616 cytometry at the indicated timepoints. An average of n=3 biological replicates is shown. Error bars
617 represent standard deviations.

618

Figure 2. Phosphosite mutations in Hcm1 decrease fitness in stress.

(A) Schematic of Phosphosite Scanning screens. Plasmids expressing all 256 mutants in the A/E library, as well as WT *HCM1*, were transformed into a strain in which expression of the genomic copy of *HCM1* is controlled by a galactose-inducible promoter. The pooled population growing in galactose was diluted and split into dextrose containing media (to shut-off expression of the endogenous copy of WT *HCM1*) with or without 150mM LiCl at the start of the experiment. (B) Scatterplot comparing average selection coefficients for each mutant in the A/E library in control and LiCl media. Pearson correlation (r) is indicated. (C-E) Box and whisker plots comparing the selection coefficients of different groups of mutants. The black center line indicates the median selection coefficient, boxes indicate the 25^{th}-75^{th} percentiles, whiskers represent 1.5 interquartile range (IQR) of the 25^{th} and 75^{th} percentile, black circles represent outliers. In all panels, selection coefficients are an average of n=4 biological replicates. (C) shows selection coefficients in cells with the indicated number of phosphomimetic mutations in control or LiCl conditions. (D-E) show selection coefficients of mutants that are either phosphodead or phosphomimetic at each position, in control (D) or LiCl containing medium (E).

Figure 3. Elevated importance of processive Hcm1 phosphorylation in stress

(A) Scatterplot comparing average selection coefficients for each mutant in the W/E library in control and LiCl media. Pearson correlation (r) is indicated. Red represents mutants that are phosphomimetic at sites T460 and S471, blue represents all other mutants. (B-F) Box and whisker plots comparing the selection coefficients of different groups of mutants. The black center line indicates the median selection coefficient, boxes indicate the 25^{th}-75^{th} percentiles, whiskers represent 1.5 interquartile range (IQR) of the 25^{th} and 75^{th} percentile, black circles represent outliers. In all panels, selection coefficients are an average of n=4 biological replicates. (B) shows selection coefficients in cells with the indicated number of phosphomimetic mutations in control

or LiCl conditions. (C-D) show selection coefficients of mutants that are either WT (S or T) or phosphomimetic at each position, in control (C) or LiCl containing medium (D). (E-F) show selection coefficients for mutants that are WT (TT) or phosphomimetic (EE) at indicated positions.

Figure 4. Dynamic phosphorylation of the Hcm1 TAD promotes fitness in stress.

(A) Diagram of Hcm1 mutant proteins showing mutated phosphosites and impacts on protein stability and phosphoregulation of the TAD region. nc, no change. (B-E) Strains with the indicated genotypes were co-cultured in control media (B, D) or media with 150mM LiCl (C, E). Percentage of each strain was quantified by flow cytometry at the indicated timepoints. An average of n=13 biological replicates is shown. Error bars represent standard deviations. (F) Comparison of selection coefficients of the indicated strains and growth conditions, from pairwise assays shown in Figures 1C, 1D, 4B, and 4C. One-way ordinary ANOVA with Šídák's multiple comparisons test was used to test significance, *p<0.0001. (G) Normalized enrichment scores (NES) of Hcm1 target genes from GSEA analysis of the indicated comparisons. Asterisk (*) indicates FDR=0.

Figure 1

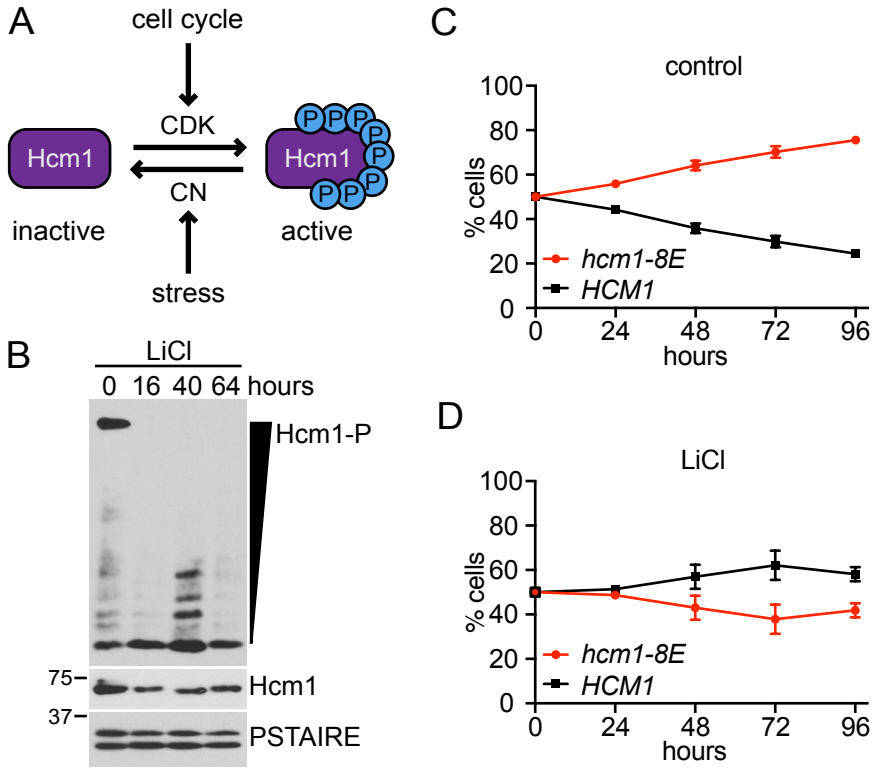

Figure 2

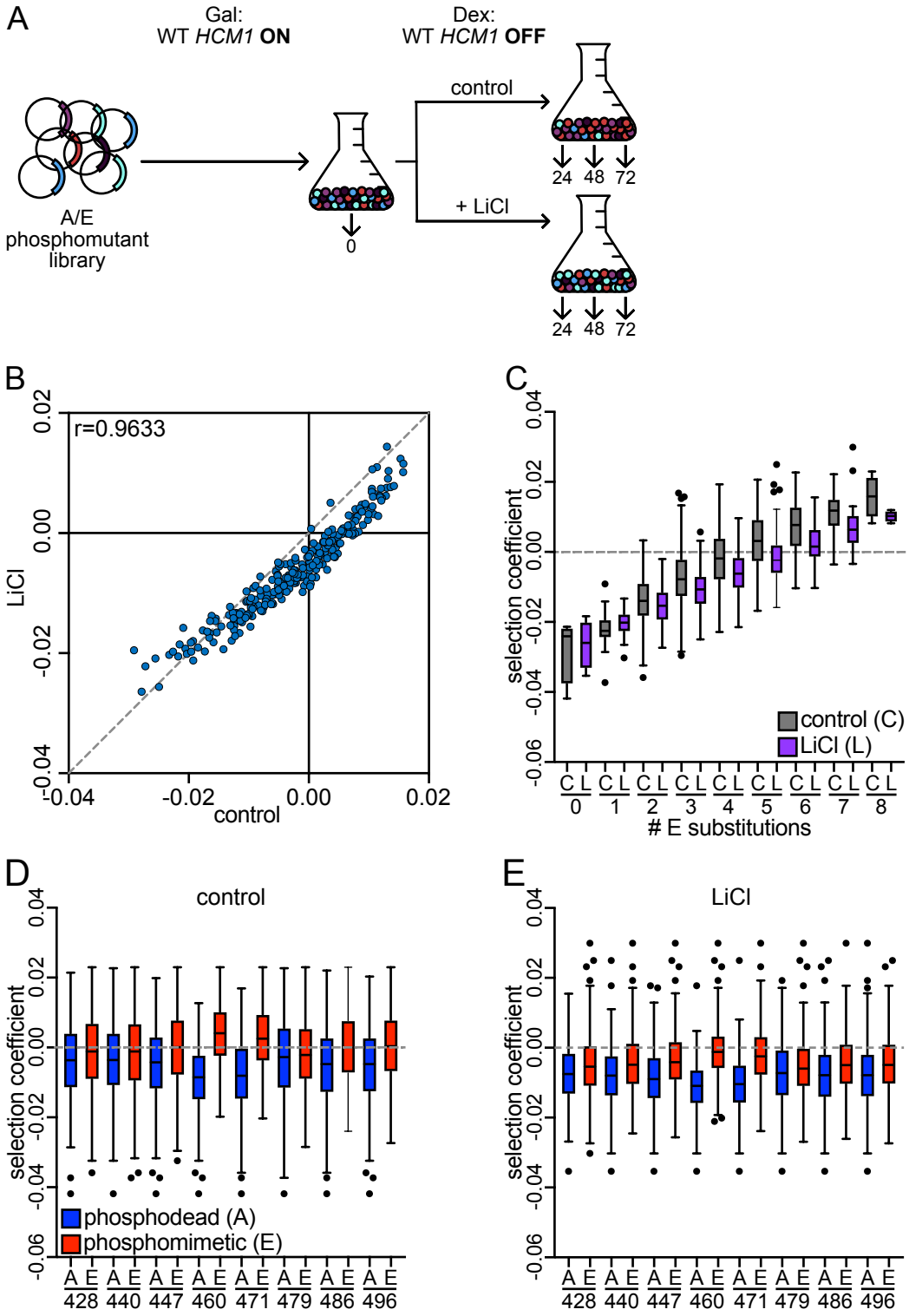

Figure 3

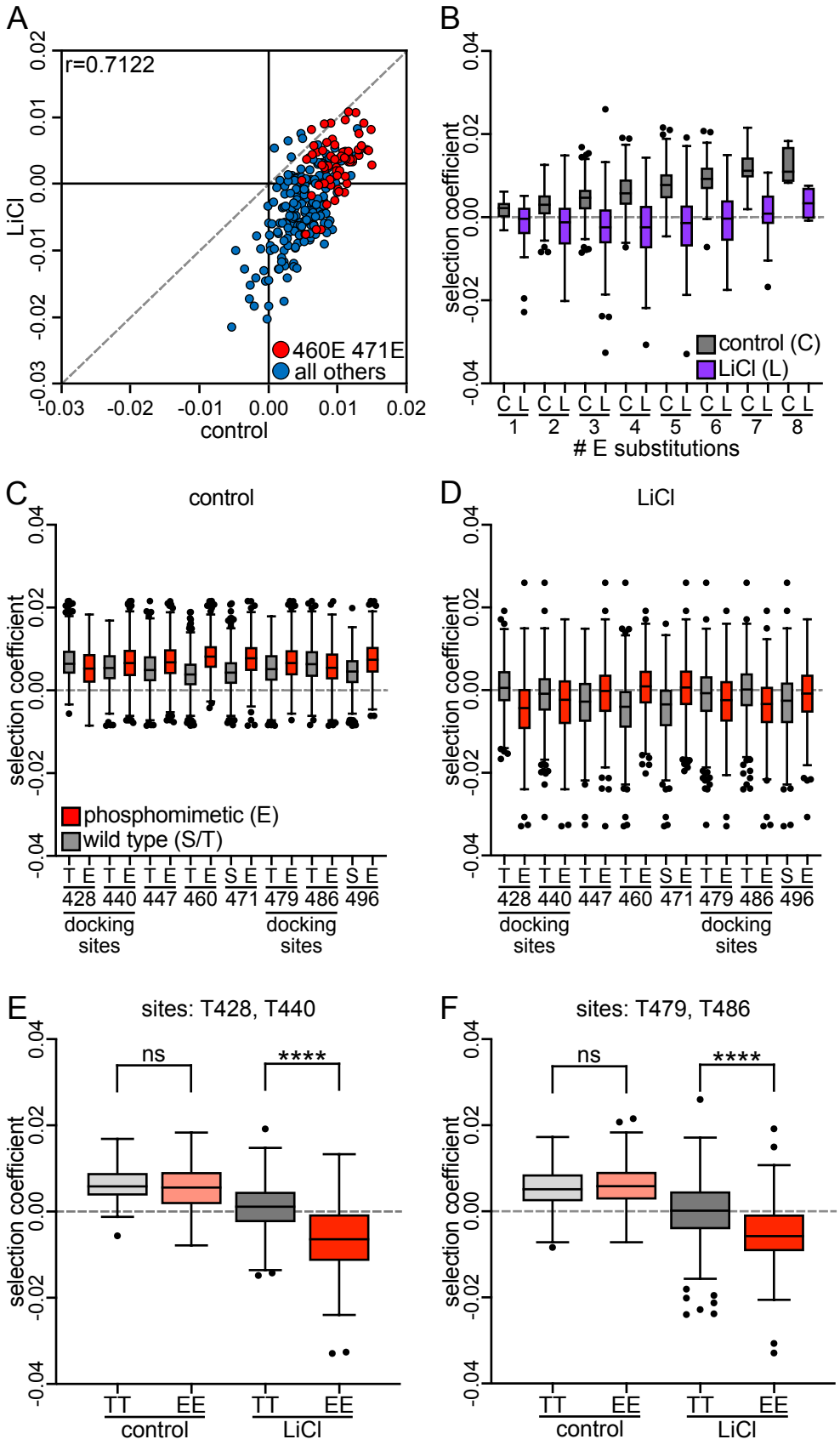

Figure 4